Learning to Focus: CSI-Free Hierarchical MARL for Reconfigurable Reflectors

Hieu Le
Electrical and Computer Engineering
Texas A&M University
College Station, Texas, USA
hieult@tamu.edu

Mostafa Ibrahim
Engineering Technology
and Industrial Distribution
Texas A&M University
College Station, Texas, USA
mostafa.ibrahim@tamu.edu

Oguz Bedir
Electrical and Computer Engineering
Texas A&M University
College Station, Texas, USA
oguzbedir@tamu.edu

Jian Tao
School of Performance,
Visualization, and Fine Arts
Texas A&M University
College Station, Texas, USA
jtao@tamu.edu

Sabit Ekin
Engineering Technology
and Industrial Distribution
Texas A&M University
College Station, Texas, USA
sabitekin@tamu.edu

arXiv:2604.05165v3 [cs.AI] 8 Sep 2026

***Abstract*—Reconfigurable Intelligent Surfaces (RIS) have the potential to engineer smart radio environments for next-generation millimeter-wave (mmWave) networks. However, the prohibitive computational overhead of Channel State Information (CSI) estimation and the dimensionality explosion inherent in centralized optimization severely hinder practical large-scale deployments. To overcome these bottlenecks, we introduce a per-element CSI-free paradigm powered by a Hierarchical Multi-Agent Reinforcement Learning (HMARL) architecture to control mechanically reconfigurable reflective surfaces. By substituting pilot-based channel estimation for each element of the device with accessible user localization data, our framework leverages spatial intelligence for macro-scale wave propagation management. The control problem is decomposed into a two-tier neural architecture: a high-level controller executes temporally extended, discrete user-to-reflector allocations, while low-level controllers autonomously optimize continuous focal points using Multi-Agent Proximal Policy Optimization (MAPPO) under a Centralized Training with Decentralized Execution (CTDE) scheme. Comprehensive deterministic ray-tracing evaluations in an indoor mmWave scenario demonstrate that this hierarchical framework achieves received signal strength indicator (RSSI) improvements of up to 7.79 dB over centralized Proximal Policy Optimization (PPO) baselines. Furthermore, the system maintains resilient beam-focusing performance under practical sub-meter localization tracking errors for up to four users and two reflector arrays. By eliminating execution-time CSI overhead while preserving high-fidelity signal redirection, this work provides a scalable and cost-effective step toward intelligent indoor wireless environments.**

***Index Terms*—Reconfigurable Intelligent Surfaces (RIS), Ray Tracing, Coverage Map, Hierarchical Multi-Agent Reinforcement Learning, Deep Reinforcement Learning**

This material is based upon work supported in part by the U.S. Department of Energy, Office of Science, Office of Advanced Scientific Computing Research, Early Career Research Program under Award Number DE-SC0023957, and in part by the National Science Foundation under Grant No. 2549088.

I. Introduction

The unprecedented surge in wireless traffic demand has driven conventional communication architectures to their theoretical limits [1]. In response, reconfigurable intelligent surfaces (RIS) have emerged as a transformative technology, turning the previously passive radio propagation medium into a dynamic, controllable environment. Conventional RIS architectures leverage electronically controlled phase shifters to induce constructive interference at receivers [1], [2]. However, these systems depend critically on accurate channel state information (CSI) for each reflecting unit [3]. As deployments scale to hundreds of elements, the pilot overhead required for cascaded channel estimation becomes a prohibitive computational bottleneck, causing high spectral efficiency loss [4].

While deep reinforcement learning (DRL) and multi-agent reinforcement learning (MARL) have been increasingly adopted to address the optimization complexity of RIS coordination, most existing frameworks still mandate explicit channel estimation [5]–[7]. Efforts to relax this CSI dependence often require massive offline training datasets or the integration of dedicated sensing hardware into the RIS, which substantially increases system cost, power consumption, and hardware complexity [8], [9].

To circumvent these fundamental limitations, we shift focus from electronic metasurfaces to mechanically reconfigurable metallic reflectors. Unlike electronic architectures that require complex RF circuitry, metallic reflectors offer inherent wideband operation and simplified mechanical actuation [10]–[12].

In our prior work, we established the physical foundation and control viability of this mechanical approach. We demonstrated that arrays of metallic flat reflectors, acting as linear Fresnel reflectors, can provide substantial coverage and gain

enhancements in non-line-of-sight (NLOS) environments, offering a low-cost, frequency-versatile alternative to electronic phase-shifters [10]. Building upon this hardware design, we introduced a MARL framework to guide these reflector arrays, demonstrating that distributed control outperforms centralized DRL baselines in multi-user scenarios [12]. However, while standard MARL mitigates the dimensionality explosion of centralized approaches, coordinating simultaneous discrete user allocation and continuous beam-focusing across massive multi-reflector environments remains a formidable computational challenge.

To overcome this remaining complexity bottleneck while leveraging the mechanical hardware, we propose a fundamentally different methodology that eliminates per-element pilot-based electromagnetic channel estimation. Instead of coordinating fine-grained electromagnetic interference, our framework exploits spatial awareness and readily available user localization data to manage macro-scale signal propagation in these NLOS environments.

While replacing per-element CSI with localization information introduces a dependency on continuous spatial tracking, acquiring high-fidelity, decimeter-level user context is highly feasible and cost-effective in modern wireless networks. Recent advancements in joint communication and sensing systems have demonstrated that commercial off-the-shelf infrastructure can provide continuous, high-update-rate localization without necessitating expensive, dedicated tracking hardware. For instance, integrated millimeter-wave radar systems have been shown to achieve robust sub-decimeter localization accuracy in dense indoor environments [13]. Furthermore, ubiquitous Wi-Fi infrastructure can now be leveraged to provide highly accurate spatial tracking and orientation data [14]. By relying on these increasingly standard sensing modalities, our framework shifts the system overhead from per-element electromagnetic channel estimation to spatial localization, which scales far more efficiently in multi-user deployments.

To manage the massive combinatorial complexity of joint user assignment and continuous control, we formulate the problem as a hierarchical multi-agent reinforcement learning (HMARL) framework [15]. The architecture decomposes the task into two temporal abstraction levels: a centralized high-level controller that performs discrete user-to-reflector allocations, and low-level controllers that autonomously optimize continuous focal points for their assigned users. Trained using multi-agent proximal policy optimization (MAPPO) [16] under a centralized training with decentralized execution (CTDE) paradigm [17], this decomposition ensures rapid learning and practical deployment scalability. Furthermore, the practical deployment viability is highly supported by the widespread availability of specialized deep learning accelerators in modern communication systems [18], [19]. Building on our prior mechanically reconfigurable reflector studies, which focused on single-level DRL control and coverage enhancement [10], [12], this work introduces an explicit hierarchical decomposition and a policy that rely on user localization and geometric priors rather than per-element CSI.

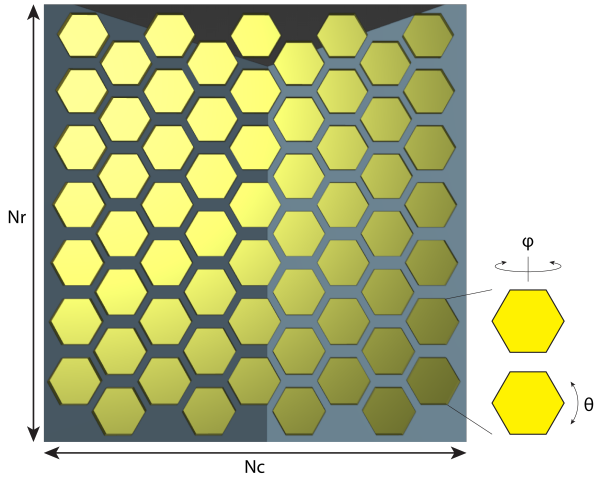

Figure 1. Reflector Design.

In this paper, we demonstrate the efficacy of this per-element CSI-free paradigm.

- **Per-element CSI-free optimization:** A fully functional HMARL framework that eliminates execution-time CSI estimation overhead, utilizing spatial localization and a pre-calibrated ray-tracing model to achieve significant received signal strength indicator (RSSI) improvements over centralized PPO baselines.
- **Hardware and algorithmic analysis:** Comprehensive ray-tracing-based validation demonstrating resilient beam focusing under practical sub-meter indoor localization errors and mechanically feasible focal-point adjustments.

II. System Model and Problem Formulation

A. Mechanically Reconfigurable Reflector & Hierarchical Coordination

The system comprises an access point (AP) located at $s \in \mathbb{R}^3$, K user equipment (UE) devices, and L independent reflector segments operating in a NLOS millimeter-wave (mmWave) environment. Unlike standard electronic phase-shifters, the reflector is a mechanical device consisting of many small metallic tiles arranged in an $N_r \times N_c$ grid (Fig. 1).

To bypass the severe computational bottleneck of per-tile optimization, we optimize for beam-focusing with a focal point so that the reflector's tiles focus energy toward that point. For a focal point $f_l(t) \in \mathbb{R}^3$ associated with reflector segment l, the mechanical orientation of tile (i, j) at position $r_{i,j}$ is deterministically governed by its normal vector:

$$\vec{n}_{i,j}(f_l) = \frac{1}{2}\left(\frac{f_l - r_{i,j}}{\|f_l - r_{i,j}\|_2} + \frac{s - r_{i,j}}{\|s - r_{i,j}\|_2}\right). \quad (1)$$

This geometric formulation allows us to derive the necessary elevation $\theta_{i,j}$ and azimuth $\phi_{i,j}$ angles without requiring instantaneous electromagnetic CSI.

To manage the massive combinatorial complexity of a multi-user, multi-reflector environment, we decompose the control problem into a two-tier HMARL architecture. There

are two levels: a high-level user–reflector assignment controller and low-level reflector focal point control agents. Operating at an extended timescale T, the high-level controller observes the global spatial state to determine the discrete user-to-reflector allocation $b = \{b_1, \ldots, b_L\}$. Given this assignment, the decentralized low-level controllers autonomously execute continuous focal-point displacements

$$a_{l,t} = [\Delta f_{l,x}, \Delta f_{l,y}, \Delta f_{l,z}]^T \tag{2}$$

at every environmental timestep to maximize the signal strength for their assigned users.

B. Signal Propagation & Optimization Objective

In the considered NLOS mmWave environment, the direct path between the AP and the users is assumed to be obstructed. Consequently, the controllable RSSI at user k relies entirely on the reflected paths facilitated by its assigned reflector segment. It is noted that we use RSSI as a proxy for link quality, defined here as the received power at each user computed from deterministic ray-tracing, expressed in dBm. For a user k assigned to segment l under the high-level allocation b, the received power is formulated as:

$$P_{r,k}(u_k, f) = P_t \sum_{(i,j)\in\mathcal{S}_{b_l}} \left| h_{r,k}^{(i,j)}(u_k, f) + h_{other,k}(u_k) \right|^2, \tag{3}$$

where P_t is the transmit power, $h_{r,k}^{(i,j)}(u_k, f)$ represents the reflected channel coefficient from tile (i, j) as a function of the user, u_k, and focal point, f, locations, and $h_{other,k}(u_k)$ accounts for other environmental propagation paths. Crucially, these coefficients are derived from deterministic ray tracing of a fixed propagation environment based on user and focal-point localization.

The system objective is to maximize the aggregate received power across all K users. We define the system-wide performance metric at time step t as a state-dependent reward function:

$$R_{sys}(s(t), b(t)) = \sum_{k=1}^{K} P_{r,k}(u_k(t), f(t)). \tag{4}$$

This formulation establishes a differentiable performance metric that directly couples the discrete high-level allocation decisions $b(t)$ with the continuous low-level focal point configurations $f_l(t)$, thus enabling coordinated hierarchical optimization.

By elevating the optimization space from individual tile orientations to segment-level focal points, the control parameter dimension is reduced from

$$\mathcal{D}_{\text{tile}} = K^L + 2N_rN_c \tag{5}$$

to a highly compact representation of

$$\mathcal{D}_{\text{focal}} = K^L + 3L. \tag{6}$$

For dense indoor deployments where the hardware complexity term $2N_rN_c$ typically dominates the segment count term $3L$, this dimensionality reduction yields the fundamental computational feasibility required for fast MARL convergence.

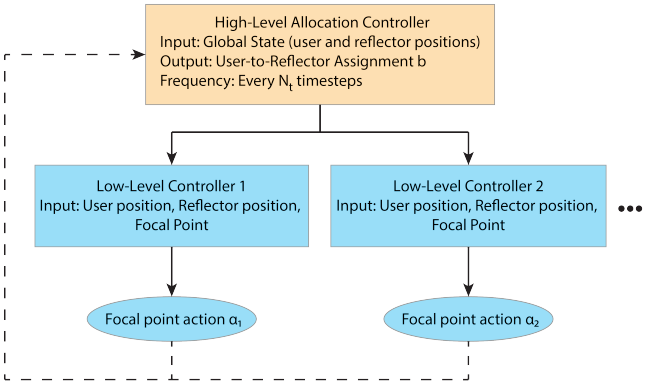

Figure 2. Hierarchical Multi-Agent Reinforcement Learning Architecture. The high-level controller evaluates the global system state to determine discrete user-to-reflector allocations every T timesteps. Concurrently, low-level agents utilize masked local observations to continuously optimize focal points using PPO under a CTDE scheme.

III. Hierarchical MARL Framework

To solve the joint optimization of user assignment and focal point placement, we formulate the problem as a Hierarchical Multi-Agent Markov Decision Process (HMA-MDP). For the HMARL, there are two distinct control levels: a high-level user–reflector assignment controller and decentralized low-level reflector focal point controllers (Fig. 2.)

A. Hierarchical Coordination Architecture

1) High-Level Allocation Controller: Operating as a centralized decision-maker, the high-level controller observes the global system state

$$s_H(t) = \{u_1(t), \ldots, u_K(t), r_1, \ldots, r_L, f_1(t), \ldots, f_L(t)\}, \tag{7}$$

to systematically evaluate user-to-reflector assignments. The controller selects a discrete combinatorial action $b(t) \in \mathcal{B}$ with cardinality $|\mathcal{B}| = K^L$. To ensure learning stability, this level operates with temporal abstraction, the controller only updates its allocation every T environmental timesteps. This extended timescale provides a stable optimization horizon, allowing the low-level controllers sufficient time to adapt their focal points before reassignment occurs, thereby preventing destructive policy oscillations.

2) Low-Level Focal Point Agents: Given an allocation b from the controller, each reflector segment l acts as an independent agent. To ensure multi-agent scalability and decouple the learning process, strict observation masking is applied. With $\pi(l)$ which allocates reflector segment to each user, each agent l executes its policy based exclusively on a localized observation.

$$o_{L,l}(t) = \{u_{\pi(l)}(t), r_l, f_l(t)\}, \tag{8}$$

which contains only the position of its assigned user, its own reflector position, and its current focal point. The agent continuously outputs displacement actions $a_{l,t} \in \mathbb{R}^3$ at every timestep, bounded by a maximum mechanical actuation

limit $\delta_{\max}$. This localized execution reduces each agent's observation space dimensionality from $\mathbb{R}^{3K+6L}$ to a reduced dimensional $\mathbb{R}^9$.

3) MAPPO with CTDE: We optimize the policies using MAPPO governed by the CTDE paradigm. During centralized training, a global critic network evaluates the complete system state s_{H} to compute accurate advantage estimates, effectively resolving the non-stationarity inherent in concurrent multi-agent updates. During deployment, the global critic is discarded, allowing the low-level controllers to execute optimal focal point adjustments purely through decentralized local observations without any inter-agent communication overhead.

B. MAPPO with CTDE and Compatibility Matrix

Both the high-level controller and the low-level focal point controllers are trained using MAPPO. To ensure stable cooperative learning, we employ a CTDE scheme. During the centralized training phase, a global critic evaluates the joint state $s_{\mathrm{H},t}$ to compute the advantage function $Adv(s_{\mathrm{H},t}, a_t^l)$, which provides accurate credit assignment and mitigates the multi-agent non-stationarity problem [16]. Each agent l then updates its policy network by maximizing the clipped surrogate objective:

$$\mathcal{L}^{\mathrm{CLIP}}(\psi_l) = \mathbb{E}_t\Big[\min\Big(r_t^l(\psi_l)\,Adv, \\ \mathrm{clip}\big(r_t^l(\psi_l), 1-\epsilon, 1+\epsilon\big)\,Adv\Big)\Big], \tag{9}$$

where $r_t^l(\psi_l)$ denotes the probability ratio of the action under the current and previous policies, $r_t^l(\psi_l) = \frac{\pi_{\psi_l}(a_t^l|o_t^l)}{\pi_{\psi_{\mathrm{old}},l}(a_t^l|o_t^l)}$ with ψ_l is the low-level controller agent l.

While the MAPPO setup ensures stable execution, the high-level allocation space still scales exponentially as K^L, creating a sparse reward landscape. Discovering near-optimal assignments through pure exploration is computationally impractical within standard training horizons. To accelerate convergence, we introduce a domain-specific compatibility matrix $C \in \mathbb{R}^{K\times L}$ that encodes prior geometric knowledge as an inductive bias.

The matrix element C_{kl} quantifies the expected signal propagation favorability when user k is assigned to reflector segment l:

$$C_{kl} = \exp\left(-\frac{\|u_k - r_l\|}{d_0}\right)\cdot\cos(\theta_{kl}), \tag{10}$$

where $\|u_k - r_l\|$ is the Euclidean distance between the user and the reflector, d_0 is a normalization constant, and θ_{kl} is the AP–reflector–user reflection angle.

Rather than acting as simple reward shaping, this matrix serves as an inductive bias injected directly into the high-level allocation policy:

$$\pi_H(b \mid s_H;\phi) \propto \left(Q_H(s_H,b) + \alpha(t)\sum_{k=1}^{K} C_{k,b_l}\right). \tag{11}$$

The coefficient $\alpha(t)$ acts as a temporal decay gate; it heavily weighs the geometric prior during the initial exploration phase and drops to zero once a predefined episode threshold is reached. This structured guidance allows the high-level controller to bypass many suboptimal combinatorial configurations, accelerating the early learning phases.

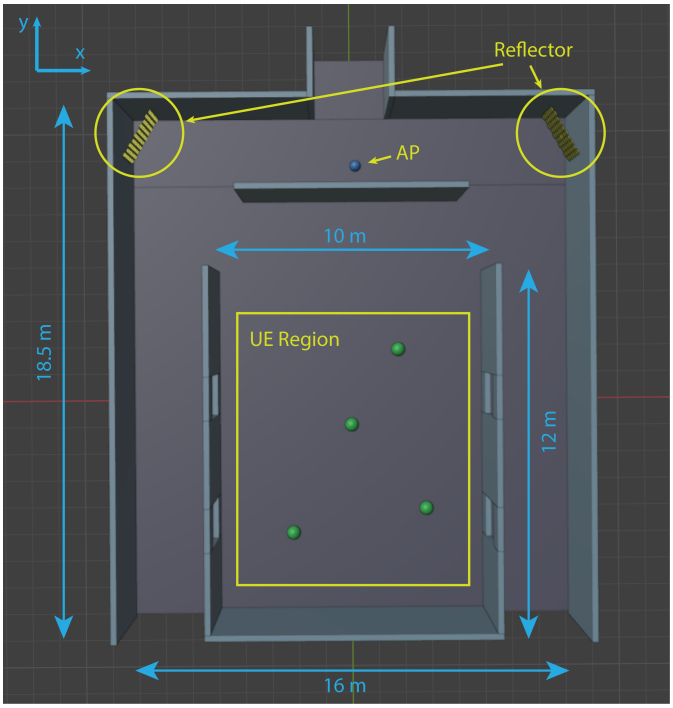

Figure 3. Experimental setup of the conference room simulation environment. The access point (AP) is positioned outside the room, serving users within the designated 10 m × 10 m coverage region. Two mechanically reconfigurable reflectors are deployed at the corners to establish NLOS links.

IV. Results and Discussion

A. Simulation Setup and Concurrent Environments

To empirically validate the proposed HMARL framework, we construct a high-fidelity 60 GHz indoor mmWave simulation environment. The experimental testbed models a conference room where an AP is positioned externally, serving K users uniformly distributed within a $10\,\mathrm{m}\times 10\,\mathrm{m}$ coverage area (Fig. 3). Two mechanically reconfigurable metallic reflector arrays are deployed at the room's corners to establish NLOS links. The total transmit power is constrained to 5 dBm to represent a low-power mmWave communication system.

Electromagnetic propagation is modeled using NVIDIA Sionna's deterministic ray-tracing engine integrated with Blender. To ensure realistic multipath phenomena, including reflections, diffractions, and scattering, structural materials are strictly parameterized according to ITU-R P.2040-1 standards. This includes concrete walls (relative permittivity, $\epsilon_r = 5.31$ and conductivity, $\sigma = 0.0326$ S/m) and marble floors ($\epsilon_r = 7.0$, $\sigma = 0.01$ S/m), while the reflector tiles are modeled as highly conductive metallic panels ($\epsilon_r = 1$).

Given the substantial computational overhead of generating ray-tracing data for millions of continuous HMARL training steps, the simulation architecture is custom-built to leverage

highly parallelized concurrent environments. We utilize multithreading to instantiate multiple simulation replicas simultaneously. Because NVIDIA Sionna is optimized for hardware acceleration, the computationally intensive ray-tracing operations are entirely offloaded to the GPU, while the CPU manages the environment logic, result gathering, and trajectory storage. By running different environment configurations in parallel and synchronously gathering the batch results at the end of each step, the framework achieves the massive sample throughput required for stable MAPPO convergence without bottlenecking the training pipeline.

Table I
SIMULATION ENVIRONMENT AND HMARL HYPERPARAMETERS

Parameter Description	**Assigned Value**
Environment & Hardware Setup	
Operating Frequency (f_c)	60 GHz
Access Point Tx Power (P_t)	5 dBm
Deployment Area	10×10 m^2
Reflector arrays & Users (K)	2 arrays; $K \in \{2, 4\}$
Policy & Value Network Architecture	
Manager Network (High-Level)	Attention + 128-unit FC (ReLU)
Agent Networks (Low-Level)	Two-layer FC (256 units, ReLU)
Optimizer	Adam
Learning Rate (η)	2.0×10^{-4}
MAPPO & Training Configurations	
Discount Factor (γ) & GAE (λ)	0.985, 0.9
PPO Clipping Ratio (ϵ)	0.2
Value Loss & Entropy Coefficients	1.0, 1.0×10^{-4}
Optimization Epochs per Batch	40 (Batch size = 200)
Total Training Episodes	3,200
Deployment Evaluation Horizon	300 timesteps
Initial Focal Point Distribution	$\mathcal{N}([0, 0, 1.5]^\top \text{m}, 2.5\mathbf{I})$

The MAPPO algorithm operates under a CTDE paradigm, where global system state information is accessible during training and at the centralized high-level controller, while individual low-level agents execute policies based solely on local observations during deployment. A complete summary of the system configuration, neural network architectures, and training hyperparameters is provided in Table I.

B. Convergence and Deployment Performance

To evaluate the learning efficiency and practical deployment viability of the proposed framework, we analyze both training convergence and post-training signal stability in a 4-user scenario. The performance of the full hierarchical framework with geometric prior (*HMARL-C*) is compared against a hierarchical variant without the compatibility matrix (*HMARL-NC*), a conventional centralized PPO agent (*Centralized*), and a random reflector–user allocation baseline (*Random*).

1) Training Convergence and the Inductive Bias: Fig. 4a illustrates the episode-averaged cumulative reward convergence over 3,000 training episodes. The *HMARL-C* method exhibits rapid initial learning, separating from the baselines within the first 500 episodes and converging to an average reward of approximately 70. In contrast, *HMARL-NC* plateaus around 51, the *Centralized* agent stabilizes near 50, and the *Random* baseline remains around 39.

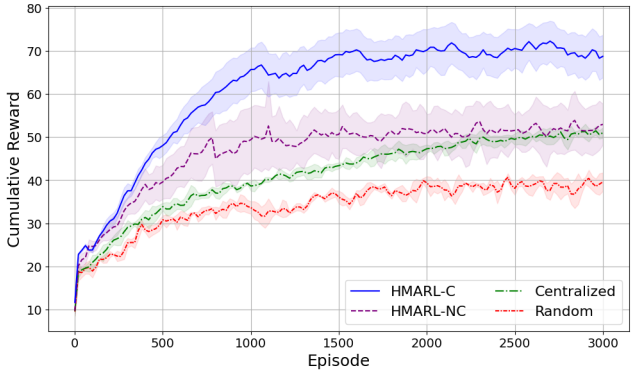

(a) Training Convergence

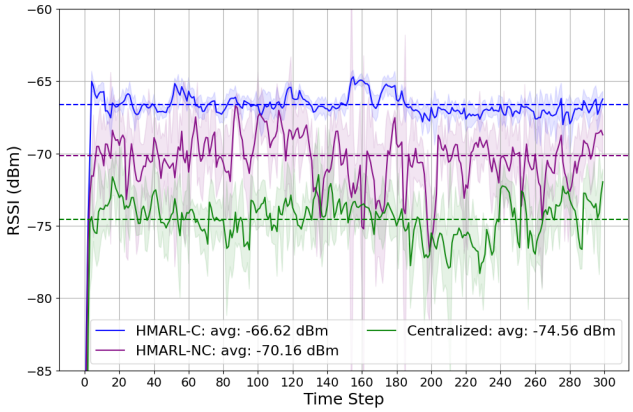

(b) Deployment RSSI

Figure 4. Performance evaluation for the 4-user configuration. (a) Cumulative reward convergence over 3,000 training episodes. (b) Deployment RSSI evaluated over 300 timesteps under continuous user mobility. Solid lines denote the mean, and shaded regions indicate the empirical standard deviation.

The performance gap between *HMARL-C* and *HMARL-NC* isolates the contribution of the domain-specific compatibility matrix. In the massive combinatorial action space of a multi-user, multi-reflector environment, discovering near-optimal assignments through pure exploration is computationally expensive. The compatibility matrix provides an essential geometric inductive bias, guiding the high-level controller toward spatially favorable configurations and helping the agents avoid convergence to suboptimal local minima.

2) Deployment RSSI and Hierarchical Improvement: To validate operational stability, the trained policies are evaluated over 300 timesteps while introducing continuous user mobility with a velocity of 1 m/s. As shown in Fig. 4b, the hierarchical architecture achieves higher RSSI than the non-hierarchical baseline methods.

The *HMARL-C* variant maintains a mean RSSI of -66.62 dBm, while *HMARL-NC* achieves -70.16 dBm and the *Centralized* agent reaches only -74.56 dBm. This corresponds to a performance gain of roughly 7.9 dB for *HMARL-C* over the centralized baseline, with *HMARL-NC* providing an intermediate improvement of about 4.4 dB. The hierarchy alone thus yields several dB gain, and the additional geometric prior further boosts RSSI and robustness under continuous

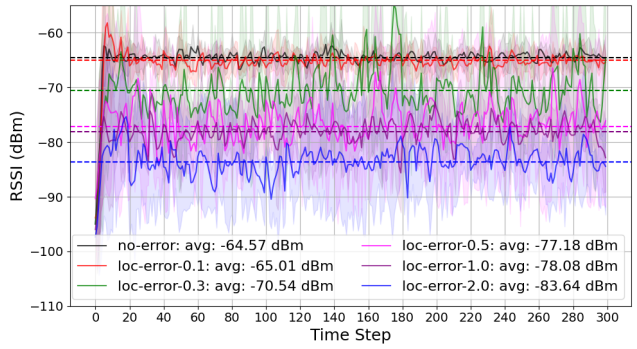

Figure 5. RSSI performance under varying degrees of user localization error for the 4-user configuration. The framework demonstrates robust, graceful degradation for sub-meter positioning noise, maintaining viable signal strength up to a 0.3 m error threshold. Solid lines represent the mean RSSI over 300 evaluation timesteps, with shaded regions denoting the empirical standard deviation.

spatial changes.

C. Sensitivity to Localization Errors

Practical deployment of the proposed per-element CSI-free hierarchical framework depends on the availability of user localization information. Real-world localization systems inevitably encounter positioning errors due to hardware limitations and environmental multipath fading, which can degrade allocation quality and beam-focusing accuracy. To evaluate the framework's practical resilience, we simulate dynamic user tracking under varying localization error levels, modeled as a zero-mean Gaussian distribution with variance $\sigma_{\text{error}} \in \{0.0, 0.1, 0.3, 0.5, 1.0, 2.0\}$ meters. The agents are trained using error-matched statistics, reflecting practical deployments where tracking system tolerances are known a priori, thereby enabling error-aware policy learning.

As illustrated in Fig. 5, the system performance exhibits a systematic and graceful degradation corresponding with the tracking error magnitude. Under ideal conditions (no error), the 4-user system maintains an average RSSI of $-64.57\,\text{dBm}$. When subjected to $0.1\,\text{m}$ errors representative of emerging Ultra-Wideband (UWB) tracking systems, the system suffers a negligible penalty of roughly $0.5\,\text{dB}$ ($-65.01\,\text{dBm}$). Operating within the $0.3\,\text{m}$ error regime, which is typical of modern commodity WiFi or Bluetooth Low Energy (BLE) positioning infrastructure, the framework successfully secures a viable $-70.54\,\text{dBm}$.

A critical operational boundary emerges at the $0.5\,\text{m}$ threshold, where performance drops to $-77.18\,\text{dBm}$ and the empirical standard deviation widens significantly. Errors exceeding $1.0\,\text{m}$ lead to severe QoS degradation (from $-78.08\,\text{dBm}$ to $-83.64\,\text{dBm}$) as the high-level controller misallocates reflectors and the continuous focal points miss their intended spatial targets. Nevertheless, by maintaining good sub-meter resilience, this evaluation confirms that the HMARL framework can be practically deployed using existing decimeter-level indoor tracking technologies. With the localization error analysis, we view the current design as most suitable for indoor or dense urban deployments where high-quality localization infrastructure is present.

D. Limitations and Future Work

While the proposed HMARL framework demonstrates high potential, the current evaluation is confined to deterministic ray-tracing simulations in specific indoor environments. First, because system performance degrades notably with localization errors exceeding 0.3 m, the framework's viability in outdoor scenarios with sparser tracking infrastructure remains an open challenge. Future work will investigate policy robustness under mismatched and non-Gaussian localization error distributions. Second, empirical validation using physical mechanical reflector prototypes and over-the-air measurements is necessary to capture real-world actuation latency and hardware imperfections. Moreover, subsequent studies will expand the evaluation scale to support massive multi-user, multi-reflector deployments.

V. Conclusion

This paper presents a HMARL framework to eliminate the prohibitive CSI estimation overhead in multi-reflector mmWave systems. By decomposing optimization into a high-level user allocator and low-level focal point controllers, the architecture leverages spatial localization and geometric priors instead of explicit per-tile CSI. Evaluations demonstrate this approach outperforms centralized baselines by up to $7.9\,\text{dB}$ and maintains robust operation under typical sub-meter localization errors. Ultimately, hierarchical learning applied to mechanically reconfigurable reflectors provides a cost-effective, wideband alternative to electronic metasurfaces for next-generation wireless environments.

References

[1] M. Di Renzo, A. Zappone, M. Debbah, M.-S. Alouini, C. Yuen, J. de Rosny, and S. Tretyakov, "Smart Radio Environments Empowered by Reconfigurable Intelligent Surfaces: How It Works, State of Research, and The Road Ahead," *IEEE Journal on Selected Areas in Communications*, vol. 38, no. 11, pp. 2450–2525, 2020.

[2] S. Zahra, L. Ma, W. Wang, J. Li, D. Chen, Y. Liu, Y. Zhou, N. Li, Y. Huang, and G. Wen, "Electromagnetic Metasurfaces and Reconfigurable Metasurfaces: A Review," *Frontiers in Physics*, vol. 8, 2021. [Online]. Available: https://www.frontiersin.org/articles/10.3389/fphy.2020.593411

[3] S. Basharat, M. Khan, M. Iqbal, U. S. Hashmi, S. A. R. Zaidi, and I. Robertson, "Exploring Reconfigurable intelligent surfaces for 6G: State-of-the-art and the road ahead," *IET Communications*, vol. 16, no. 13, pp. 1458–1474, 2022. [Online]. Available: https://ietresearch.onlinelibrary.wiley.com/doi/abs/10.1049/cmu2.12364

[4] C. Hu, L. Dai, S. Han, and X. Wang, "Two-Timescale Channel Estimation for Reconfigurable Intelligent Surface Aided Wireless Communications," *IEEE Transactions on Communications*, vol. 69, no. 11, pp. 7736–7747, 2021.

[5] C. Huang, R. Mo, and C. Yuen, "Reconfigurable Intelligent Surface Assisted Multiuser MISO Systems Exploiting Deep Reinforcement Learning," *IEEE Journal on Selected Areas in Communications*, vol. 38, no. 8, pp. 1839–1850, 2020.

[6] A. Taha, Y. Zhang, F. B. Mismar, and A. Alkhateeb, "Deep Reinforcement Learning for Intelligent Reflecting Surfaces: Towards Standalone Operation," in *2020 IEEE 21st International Workshop on Signal Processing Advances in Wireless Communications (SPAWC)*, 2020, pp. 1–5.

[7] A. Taha, M. Alrabeiah, and A. Alkhateeb, "Enabling Large Intelligent Surfaces With Compressive Sensing and Deep Learning," *IEEE Access*, vol. 9, pp. 44 304–44 321, 2021.

[8] H. Choi, L. V. Nguyen, J. Choi, and A. L. Swindlehurst, "A Deep Reinforcement Learning Approach for Autonomous Reconfigurable Intelligent Surfaces," in *2024 IEEE International Conference on Communications Workshops (ICC Workshops)*, 2024, pp. 208–213.

[9] B. Sheen, J. Yang, X. Feng, and M. M. U. Chowdhury, "A Deep Learning Based Modeling of Reconfigurable Intelligent Surface Assisted Wireless Communications for Phase Shift Configuration," *IEEE Open Journal of the Communications Society*, vol. 2, pp. 262–272, 2021.

[10] H. Le, O. Bedir, M. Ibrahim, J. Tao, and S. Ekin, "Guiding Wireless Signals with Arrays of Metallic Linear Fresnel Reflectors: A Low-cost, Frequency-versatile, and Practical Approach," in *2024 IEEE 100th Vehicular Technology Conference (VTC2024-Fall)*, 2024, pp. 1–7.

[11] W. Khawaja, O. Ozdemir, Y. Yapici, F. Erden, and I. Guvenc, "Coverage Enhancement for NLOS mmWave Links Using Passive Reflectors," *IEEE Open Journal of the Communications Society*, vol. 1, pp. 263–281, 2020.

[12] H. Le, O. Bedir, M. Ibrahim, J. Tao, and S. Ekin, "Signal Whisperers: Enhancing Wireless Reception Using DRL-Guided Reflector Arrays," *IEEE Transactions on Machine Learning in Communications and Networking*, vol. 4, pp. 265–281, 2026.

[13] G. Zhang, G. Chi, Y. Zhang, X. Ding, and Z. Yang, "Push the limit of millimeter-wave radar localization," *ACM Transactions on Sensor Networks*, vol. 19, no. 3, pp. 1–21, 2023.

[14] G. Chi, Z. Yang, J. Xu, C. Wu, J. Zhang, J. Liang, and Y. Liu, "Wi-Drone: Wi-Fi-based 6-DoF tracking for indoor drone flight control," in *Proceedings of the 20th Annual International Conference on Mobile Systems, Applications and Services (MobiSys)*, 2022, pp. 56–68.

[15] R. Makar, S. Mahadevan, and M. Ghavamzadeh, "Hierarchical Multi-Agent Reinforcement Learning," in *Proceedings of the Fifth International Conference on Autonomous Agents*, 2001, pp. 246–253.

[16] C. Yu, A. Velu, E. Vinitsky, J. Gao, Y. Wang, A. Bayen, and Y. Wu, "The Surprising Effectiveness of PPO in Cooperative Multi-agent Games," *Advances in Neural Information Processing Systems*, vol. 35, pp. 24 611–24 624, 2022.

[17] L. Kraemer and B. Banerjee, "Multi-agent reinforcement learning as a rehearsal for decentralized planning," *Neurocomputing*, vol. 190, pp. 82–94, 2016.

[18] A. Nasari, H. Le, R. Lawrence, Z. He, X. Yang, M. Krell, A. Tsyplikhin, M. Tatineni, T. Cockerill, L. Perez, D. Chakravorty, and H. Liu, "Benchmarking the Performance of Accelerators on National Cyberinfrastructure Resources for Artificial Intelligence / Machine Learning Workloads," in *Practice and Experience in Advanced Research Computing 2022: Revolutionary: Computing, Connections, You*, ser. PEARC '22. New York, NY, USA: Association for Computing Machinery, 2022. [Online]. Available: https://doi.org/10.1145/3491418.3530772

[19] H. Le, Z. He, M. Le, D. Chakravorty, L. M. Perez, A. Chilumuru, Y. Yao, and J. Chen, "Insight Gained from Migrating a Machine Learning Model to Intelligence Processing Units," in *Practice and Experience in Advanced Research Computing 2024: Human Powered Computing*, ser. PEARC '24. New York, NY, USA: Association for Computing Machinery, 2024. [Online]. Available: https://doi.org/10.1145/3626203.3670527